Unsaturated Soils – Buzzi, Fityus & Sheng (eds)
© 2010 Taylor & Francis Group, London, ISBN 978-0-415-80480-6

The mega South-to-North Water Transfer Project in China – Unsaturated soil mechanics aspects

C.W.W. Ng & J. Xu
Department of Civil & Environmental Engineering, The Hong Kong University of Science and Technology, HKSAR, PR China

L.T. Zhan
Department of Civil Engineering, Zhejiang University, Hangzhou, PR China

ABSTRACT: The design and construction of the middle-route of China's mega South-to-North Water Transfer Project (SNWTP) has been started. The 1,427 km middle-route project is expected to transport potable water from the Yangtze River to Beijing. A canal with a trapezoidal cross-section formed by cut and fill slopes is proposed. The potential instability of these slopes passing through about 340 km unsaturated expansive soil zones imposes a major geotechnical challenge on the design and construction of the middle-route. A typical expansive soil cut slope, with and without grass cover, was therefore selected for a comprehensive and well-instrumented field study of the effects of rainfall infiltration. Artificial rainfall events were created during the field study. The performance of the slope in response to the changes in two independent stress variables (i.e., net stress and suction) was studied. The responses of a bare area and a grassed area on the selected slope were monitored and the influences of vegetation were investigated.

1 INTRODUCTION

Water scarcity is a matter of worldwide concern and it is also plaguing China today. With 22% of the world's population, China has access to only 8% of the world's fresh water supply. Its per capita availability of fresh water is barely a quarter of the world average. The uneven distribution of water resources in China has aggravated this problem. The north accounts for 37% of the country's total population and 45% of cultivated land, but only 12% of the total water resources are found there. Over 80% direct water runoff in China takes place in the south.

A mega infrastructure project, the South-to-North Water Transfer Project (SNWTP), has been proposed to respond to China's water scarcity and uneven water distribution problems. The SNWTP is proposed to carry potable water from the Yangtze River region in the south to many arid and semi-arid areas in the northern regions of China. It is the largest hydraulic project in the world. Three water transport routes have been proposed for the SNWTP, i.e., the western-route, middle-route and eastern-route. The planned construction period for the entire SNWTP will be about 50 years. The western-route is located in the western region where the Yangtze River and Yellow River headwaters are closest to one another. The eastern-route follows the course of the Grand Canal. The middle-route is from the upper reaches of the Han River (a tributary of the Yangtze River) to Beijing and Tianjin. Its approximate route is shown in Figure 1 (Ng et al. 2003). The proposed 1427 km middle-route of the SNWTP is likely to be an open-channel canal with a trapezoidal cross-section formed by cut slopes and fills. Figure 2 shows a photograph of the intake canal of the SNWTP (middle-route).

About 340 km of the proposed excavated canal passes through areas of unsaturated expansive soils. Expansive soil is a kind of soil that has a potential for swelling due to an increase in water content (Nelson &

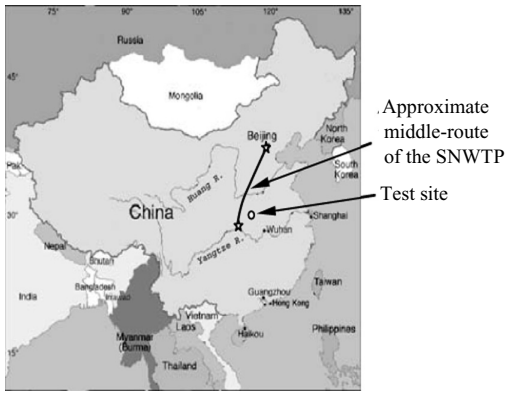

Figure 1. Approximate middle-route of the SNWTP and the test site location (Ng et al. 2003).

Figure 2. Intake canal of the SNWTP (middle-route).

Figure 3. A typical failure of an expansive soil slope at Dagangpo (Zhan 2003).

Figure 4. A typical shallow retrogressive slope failure at Dagangpo (Zhan 2003).

Miller 1992). The swelling in expansive soil is mainly due to the presence of active clay minerals such as montmorillonite. Expansive soil is widely distributed in the world and has been found in more than 40 counties and regions. It is generally in an unsaturated state. Expansive soil often causes damage to light buildings, pavement and slopes. Destruction caused by this type of soil have been reported in many countries around the world, e.g., the United States, Australia, South Africa, India, Canada, China and Israel (Nelson & Miller 1992, Steinberg 1998). According to Steinberg (1998), the annual loss from damages caused by expansive soil is US$10 billion and up to ¥100 million in the United States and China, respectively. This is far more than the total annual losses caused by floods, earthquakes and windstorms. Therefore, there is an urgent need to improve our understanding of the fundamental behaviour of unsaturated expansive soil and to improve design methodologies for civil engineering structures constructed on this type of soil (Bao & Ng 2000).

One of the major geotechnical problems associated with the SNWTP middle-route canal is the failure of expansive soil slopes, particularly failure of shallow retrogressive slopes. Figure 3 shows a typical failure of an expansive soil slope at Dagangpo in Zhaoyang, Hubei, China (Zhan 2003). Figure 4 shows typical shallow retrogressive slope failures in expansive soil at Dagangpo. Slope instability, particularly relatively shallow retrogressive type landslides, related to the expansion and shrinkage of the unsaturated expansive soils, results from changes in the soil suction during wetting and drying seasons. Hence, these expansive soils have created problems for infrastructure development in the region.

It is generally recognized that a number of landslides in unsaturated soils are triggered by rainfall infiltration during wet seasons (Fredlund & Rahardjo 1993, Lim et al. 1996). Bao & Ng (2000) pointed out that lateral unloading due to excavation and rainfall infiltration during wet seasons were two crucial external factors inducing landslides in unsaturated expansive soils. Field instrumentation and monitoring to study the effects of rainfall infiltration on slope stability have been carried out extensively on non-expansive soils, particularly residual soils (Affendi & Faisal 1994, Lim et al. 1996, Gasmo et al. 1999). However, the behaviour of an expansive soil is somewhat different from that of a residual soil. Expansive soil exhibits significant swelling or shrinkage upon wetting or drying. It has an abundance of cracks and fissures due to alternative swelling and shrinking with climate changes. In addition, it is generally over-consolidated or highly over-consolidated due to desiccation. Bao & Ng (2000) pointed out that the abundant cracks developed in unsaturated expansive soil are a key internal factor leading to landslides along crack-extension surfaces. Field investigation of rain-induced slope failure in unsaturated expansive soils is relatively rare in the literature. Some exceptions are Ortigao et al. (1997) and Liu (1997). However, the fundamental mechanisms of rainfall infiltration into unsaturated expansive soils during wet seasons have not been fully understood. In particular, the complex interaction between the variations of two independent stress

state variables (soil suction and net stress) has rarely been studied and reported. In addition, the effects of vegetation have not been investigated thoroughly.

To improve our understanding of the fundamental mechanisms of rainfall-induced landslides in unsaturated expansive soils, an 11 m high cut slope in a typical medium-plastic expansive clay in Zaoyang, close to the middle-route of the SNWTP in Hubei, China, was selected for a comprehensive well-instrumented field study. Based on Ng et al. (2003), Ng & Zhan (2007) and Zhan et al. (2007), some key monitored responses of the unsaturated expansive soil slope due to changes in both suction and net stress, with and without vegetation, are described and summarized in this paper.

2 THE TEST SITE

The test site was located on the intake canal of the Dagangpo second-level pumping station in Zaoyang, Hubei, China. It was about 230 km northwest of Wuhan and about 70 km south of the intake canal for the SNWTP in Nanyang, Henan. The location of the test site is shown in Figure 1. The site was located in a semi-arid area with an average annual rainfall of about 800 mm with 70% of the annual rainfall is occurring between May and September.

The intake canal at the test site was excavated in 1970 with an average excavation depth of 13 m. Several years after construction of the intake canal, a number of slope failures took place in succession and parts of a masonry retaining wall were seriously deflected or destroyed. Most of the mass movement occurred during wet seasons and the slip surfaces were on the order of 2 m deep. Just to the west of the selected test areas, there were a number of typical shallow slips and retrogressive slope failures, as shown in Figure 4.

The test site was selected on a cut slope on the northern side of the canal, as shown in Figure 5. The test site consisted of two neighbouring monitoring areas (both 16 m wide by about 30 m long): namely a bare area and a grassed area. The bare and grassed areas may represent surface cover conditions of the real slope under different climatic conditions, such as winter and summer. The slope had an inclination angle of 22° and a height of 11 m (measured from the top of the retaining wall). The ground level at the toe of the slope was approximately +96-m OD (Ordinary Datum). About 5 m away from the slope toe, there was a 3 m high masonry retaining wall. The depth of the canal below the slope toe was about 3.5 m. There was a 1 m wide berm at the mid-height of the slope, dividing the slope into upper and lower parts. The selected test areas had a significant depth of typical unsaturated expansive soil. The slope surface was originally grassed but no trees were present. The types of grass mainly included weed and couch grass and their heights ranged from 100 to 500 mm. The depths of roots observed on an excavated face ranged from 100 to 300 mm. The bare area was obtained by removing the top soil to a depth of about 100 mm.

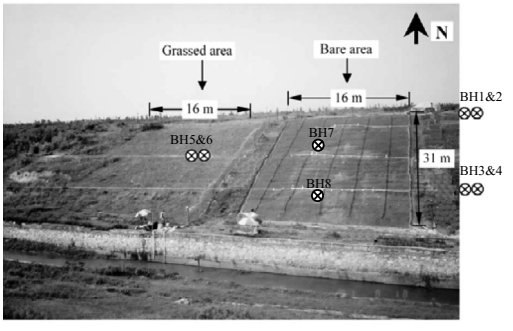

Figure 5. Full view of the cut slope and relative locations of the boreholes (modified from Ng & Zhan 2007).

3 SOIL PROFILE AND PROPERTIES

Prior to instrumentation, site investigation was carried out on the selected slope to investigate the ground conditions. The site investigation mainly consisted of borehole investigation and double-ring infiltration tests. Sampling, standard penetration tests (SPT) and dilatometer tests (DMT) were conducted in the boreholes (Ng et al. 2003, Zhan et al. 2007). The relative locations of the boreholes are shown in Figure 5. Three groups of boreholes were drilled into a layer with hard and coarse calcareous concretions around the bare area on the slope. Each group comprised two boreholes spaced 1 m apart. The three groups of boreholes BH1&2, BH5&6 and BH3&4 were located at the upper, middle and lower parts of the slope, respectively. One borehole in each group was for sampling and standard penetration tests (SPT), and the other was for dilatometer tests (DMT). Another two boreholes, BH7&BH8, were drilled in the bare area and used for the installation of inclinometers after sampling and SPTs.

The soil profiles and geotechnical parameters obtained from the boreholes near the mid-slope (BH5&6) are shown in Figure 6 (Ng & Zhan 2007). The geotechnical parameters include water content (w), dry density (ρ_d), SPT N value, undrained shear strength (c_u) and K_0 value from DMT (K_{0DMT}). The predominant stratum below the slope surface was a brown-yellow mottled gray clay. The clay layer was sometimes interlayered with thin layers of gray clay or iron concretions. X-ray diffraction analyses indicated that the predominant clay minerals were illite (31%–35%) and montmorillonite (16–22%), with a small percentage of kaolinite (8%) (Liu 1997). Some

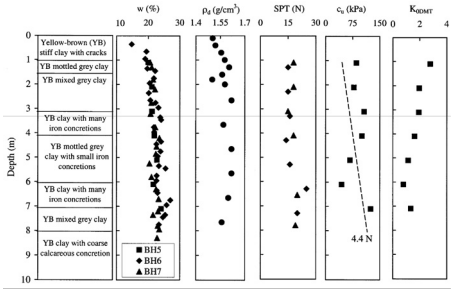

Figure 6. Soil profiles and geotechnical parameters from the boreholes at mid-slope (Ng & Zhan 2007).

Table 1. Typical properties of natural expansive clay.

Soil properties	Clay content (≤0.002 mm) (%)	Liquid limit (%)	Plastic limit (%)	Swelling pressure (kPa)	1-D free swelling (%)
Values	30–45	50–60	18–25	30–200	1–10

typical properties of the natural expansive clay are listed in Table 1. The expansive clay was silty clay with an intermediate plasticity and a medium expansive potential. The clay was over-consolidated due to desiccation, as indicated by the total stress K_0 value obtained from dilatometer tests and its swelling pressure, which ranged from 30 to 200 kPa.

The upper soil layer with a thickness varying from 1.0 to 1.5 m was rich in cracks and fissures, particularly at the upper part of the overall slope. The maximum width of the open cracks was about 10 mm. The width of the cracks decreased with an increase in depth. The maximum depth of the open cracks was estimated to be approximately 1.2 m. The soil also contained a variety of narrower cracks. The abundance of cracks and fissures was mainly attributed to the desiccation of the expansive clay during dry seasons.

During the site investigation, double-ring infiltration tests were carried out at the site to investigate the infiltration characteristics of the soil layer near the ground surface. Figure 7 shows the changes in the infiltration rate in relation to time in two different ground conditions: one infiltration test in an area abundant with open cracks and the other without obvious open cracks. The infiltration rate is defined as the amount of water per surface area and unit time penetrating into the soil. It should be noted that the infiltration rate is different from conductivity even though the units are similar. The measured infiltration rate in the ground without obvious open cracks was distinctly low, on the order of 10^{-7} m/s or less. The gradual decrease in the infiltration rate during the first two days of the test was probably due to a decrease in the hydraulic gradient resulting from a loss of soil suction upon wetting. In the cracked ground, the infiltration rate measured within the first one to two hours was quite large, on the order of 10^{-4} m/s. This was attributed to the rapid ingress of water into the open cracks. The infiltration rate decreased dramatically with test duration during the first half day and then tended towards a steady value. The main reason for the sharp decrease in the infiltration rate appears to be related to the water storage capacity of the open crack channels. These cracks tended to close with time due to soil swelling upon wetting. Favre et al. (1997) also reported that high intensity rain falling onto a dry and cracked soil resulted in rapid crack closure at the soil surface within 4.5 hours due to swelling of unsaturated soils, and that the bypass flow processes were a matter of several hours only.

As shown in Figure 7, the infiltration rate at equilibrium in the ground with open cracks is always greater than that in the ground without open cracks. The final infiltration rate in the ground with open cracks is close to the initial infiltration rate in the ground without open cracks. The observed difference in the infiltration rate between the two different ground surface conditions is basically consistent with the field measurements obtained by Øygarden et al. (1997). They found that measured values of hydraulic conductivity on site varied by three orders of magnitude from 10^{-4} to 10^{-7} m/s due to the variability of cracks.

Figure 8 shows the *in-situ* relationship between water content and matric suction, along with the soil-water characteristic curves (SWCCs) measured

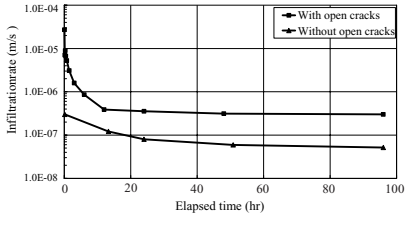

Figure 7. Changes in the infiltration rate in relation to time from a double-ring infiltration test (Zhan et al. 2007).

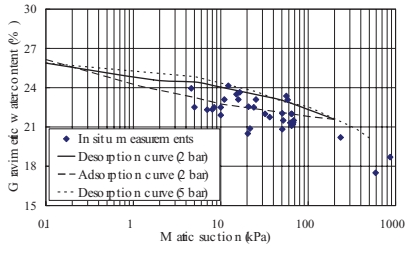

Figure 8. Relationships between water content and matric suction obtained from *in-situ* and laboratory measurements (Zhan et al. 2006).

in the laboratory. SWCCs for the natural expansive clay were measured on the specimens trimmed from the block samples taken from the test site at a depth of 1 m. The SWCCs were measured by using a 5-bar pressure plate and a 2-bar volumetric extractor. It can be seen that the shape of the SWCCs for the expansive soil is relatively flat, which indicates that the expansive clay possesses a high water retention ability within the suction range considered (0 to 500 kPa). The hysteresis between the desorption and adsorption curves appears to be relatively insignificant, probably because natural specimens have experienced many wetting/drying cycles in the field. Similar results on other natural soils were reported in the literature (Ng & Pang 2000). Although the data points from the *in-situ* measurements are relatively scattered, the average value seems to be close to the adsorption curve of the SWCC.

4 INSTRUMENTATION AND RAINFALL SIMULATION

4.1 *Instrumentation program*

Two neighbouring areas were selected on the cut slope for instrumentation as shown in Figure 5. Prior to instrumentation, the grass in the eastern area (16 m wide by 31 m long) was cleared. However, the grass in the western area (16 m wide by 28 m long) was kept. Hence, the eastern and western areas were termed as the bare and grassed areas, respectively. The layout of instrumentation in both the bare and grassed areas is shown in Figures 9. The cross section of the instrumented slope is shown in Figure 10. The main objective of the field study in the bare area was to investigate the fundamental rainfall infiltration mechanism and the complex interaction among the changes in soil suction (or water content), *in-situ* stress state and soil deformation in the unsaturated expansive soil slope. The instrumentation in the bare area was very comprehensive, including jet-filled tensiometers, thermal conductivity suction sensors (Fredlund et al. 2000), Theta-probes for determining water content (Thetaprobe 1999), vibrating-wire earth pressure cells, inclinometers, movement points, a tipping bucket rain gauge, a vee-notch flow meter and an evaporimeter. The purpose of the study in the grassed area was to investigate the influence of vegetation on rainfall infiltration and hence on soil suction and water contents in the unsaturated expansive soil. The instruments in the grassed area include jet-filled tensiometers, Theta-probes, a tipping bucket rain gauge and a vee-notch flow meter. Except for the inclinometers and movement points, all other instruments were connected to the computerised data acquisition system for data collection.

4.1.1 *Monitoring the soil suction and water content*

As shown in Figure 9, there were three rows of instrumentation for soil suction and water content monitoring in both the bare and grassed areas, i.e., R1 at the upper part, R2 at the middle part and R3 at the lower part of the slope. Jet-filled tensiometers were used

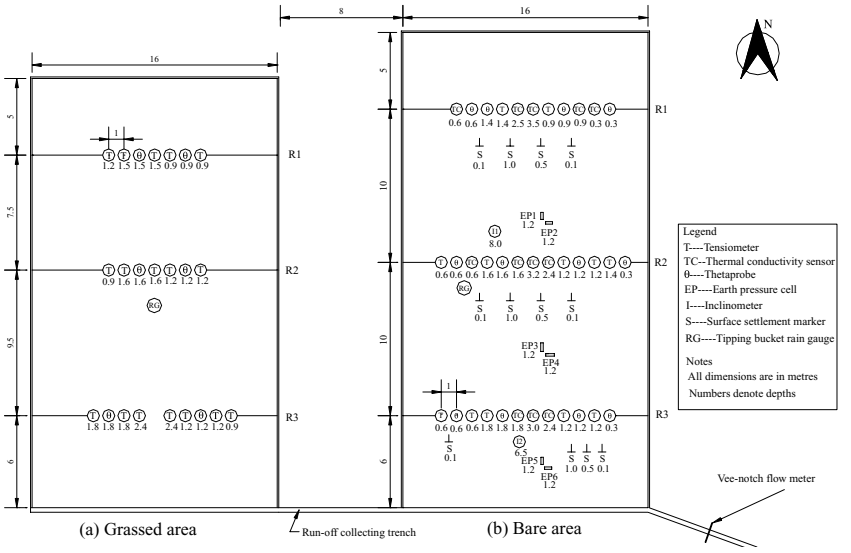

Figure 9. Layout of instruments on the expansive soil slope in: (a) Grassed area and (b) Bare area (modified from Ng et al. 2003, Ng & Zhan 2007).

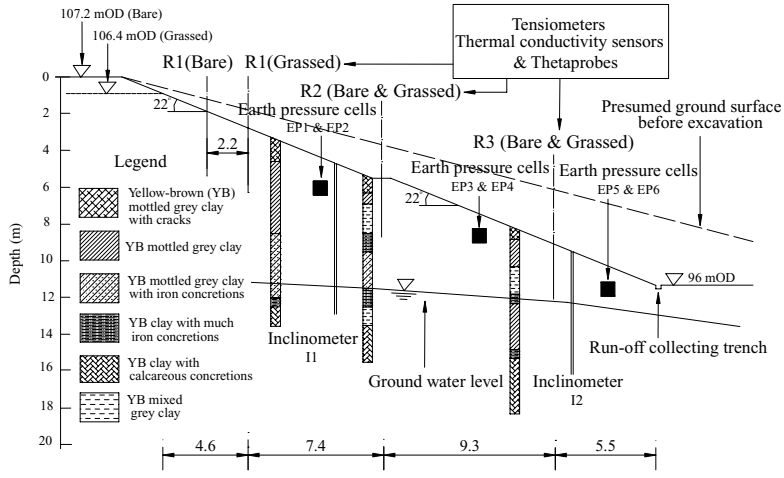

Figure 10. Cross section of the instrumented slope (modified from Ng et al. 2003, Ng & Zhan 2007).

to measure negative pore-water pressure in the slope. Since the measuring range of tensiometers is generally less than 90 kPa due to cavitation, thermal conductivity sensors were used for higher suction measurements. Thermal conductivity sensors could produce a reasonably reliable measurement of soil suction over a relatively wide range (i.e., 5 to 1500 kPa) and over a long period of time without servicing. Theta-probes were installed for monitoring volumetric water contents of the soil. Theta-probes use the standing wave technique to measure the apparent dielectric constant of a soil, which is then correlated with the volumetric water content of the soil.

In the bare area, 12 jet-filled tensiometers, 12 thermal conductivity suction sensors and 12 Theta-probes were installed. As shown in Figure 9b, in each row, seven to nine suction sensors (jet-filled tensiometers or thermal conductivity sensors) and four Theta-probes were installed and spaced 1 m apart. Most of the sensors were embedded within the top 2 m, because the depth of infiltration was likely to be no more than 2 m according to the double-ring infiltration test results. At each depth, there were generally two soil suction sensors and one Theta-probe, so that the measured data from the three sensors could be verified with each other. In the grassed area, 17 jet-filled tensiometers were installed at depths greater than 0.9 m since the initial soil suction near the ground surface was estimated to exceed the measuring range of a tensiometer. As shown in Figure 9a, in each row, five to seven jet-filled tensiometers and two Theta-probes were installed and spaced 1 m apart.

In both areas, disturbed samples were taken to measure the variations of gravimetric water content profiles during the rainfalls. Disturbed samples were taken slightly below the three rows of instrumentation using a small-diameter auger. All the auger holes were backfilled immediately after sampling.

4.1.2 *Monitoring horizontal total stress*

Three pairs of vibrating-wire earth pressure cells were installed for monitoring horizontal total stress in two orthogonal directions in the bare area, as shown in Figures 9b and 10. A mid-slope berm divided the slope into two parts. A pair of earth pressure cells (EP1&2) was embedded 2.5 m above the berm in the upper half portion of the slope. A pair of earth pressure cells (EP5&6) was installed 2.5 m above the toe in the lower half portion of the slope. The other pair of earth pressure cells (EP3&4) was located midway between the former two pairs. In each pair, one earth pressure cell was installed to measure the horizontal stress in the North-South direction (i.e., the inclination direction of the slope), while the other was placed in the East-West direction (i.e., the longitudinal direction of the canal). All six earth pressure cells were installed vertically at a depth of 1.2 m. The earth pressure cells used in this study were of the hydraulic type. Both compression stress and tensile stress could be recorded. The installation procedure proposed by Brackley & Sanders (1992) was adopted to minimize soil disturbance due to the excavation of the slot for a pressure cell. During installation, the clearance between the wall of the earth pressure cell and the soil was backfilled with an epoxy resin. The thin layer of epoxy resin adhered the cell securely to the soil and it allowed transmission of tensile force between the cell and the soil. The monitored results by Brackley & Sanders (1992) demonstrated that a tensile force could be detected by vibrating-wire earth pressure cell.

4.1.3 *Monitoring horizontal movement and surface heave*

The horizontal movement and surface heave were only measured in the bare area. Horizontal displacements of the ground were monitored manually by measuring the tilting along two inclinometer tubes. Two inclinometers were installed in two orthogonal directions to measure horizontal movement of the ground. One inclinometer (I1) was installed near the berm in the upper half portion of the slope. The other inclinometer (I2) was embedded near the toe of the lower half portion of the slope. The inclinometers were installed down to the hard layer with coarse and hard calcareous concretions. The upper (I1) and lower (I2) inclinometers were bottomed at depths of 8.0 m and 6.5 m, respectively.

To measure the swelling of the unsaturated expansive soil as a result of rainwater infiltration, three rows of movement points were set up near the three main rows of instrumentation (R1, R2 and R3) in the bare area, labelled as S in Figure 9b. The movement points were constructed with concrete blocks. Each row had four movement points founded at depths of 0.1, 0.1, 0.5 and 1.0 m. Two levelling datum points were constructed 20 m outside the artificial rainfall area and founded at a depth of 3 m. These two datum points were frequently monitored and checked using a city grid datum located over 100 m away from the test site. The monitoring and checking confirmed that the two datum points were stable and were not affected by the artificial rainfalls.

4.1.4 *Monitoring rainfall intensity, runoff and evaporation*

A tipping-bucket rain gauge was installed in each area to record the intensity and duration of the rainfall, as shown in Figure 9. Flow meters were installed in the main water-supply line of a sprinkler system to record the total amount of water sprinkled onto the slope within a given time interval. A water collection trench was constructed along the toe of the slope to measure the surface runoff using a vee-notch flow meter installed at the end of the trench. An evaporimeter was installed at mid-slope outside the monitoring area to measure the daily evaporation potential from the free water surface.

4.2 *Rainfall simulation*

Artificial rainfall was produced to accelerate the field test program. Rainfall was produced artificially using a purpose-designed sprinkler system. The sprinkler system mainly comprised a pump, a main water-supply line, three groups of branch pipes, 35 sprinkler heads and accessories. The sprinkler heads for the three groups of branch pipes were arranged such that a relatively uniform rainfall could be produced. The system could produce three levels of rainfall intensity, approximately 3, 6 and 9 mm/hr. The three levels of rainfall were regulated via the three flow-rate controlling valves. The lowest, medium and highest levels of rainfall intensity were controlled by opening one group, two groups and three groups of branch pipes, respectively. In this field study, the lowest level of rainfall intensity was used for the rainfall simulation because the water permeability of the expansive clay is relatively low, on the order of 10^{-7} m/s.

Prior to the commencement of the field study (i.e., 1 June 2001), the test site had experienced about seven months of drought with a total rainfall of less than 100 mm. After 1 June, the bare area was covered with a plastic membrane until the commencement of the simulated rainfall on 18 August. Figure 11 shows the simulated rainfall events in both the bare and the grassed areas during the monitoring period. Two rainfall events were simulated in the bare area. The first one lasted for seven days, from the morning of 18 August to the morning of 25 August, with an average daily rainfall of 62 mm. The second simulated rainfall was from the morning of 8 September to the afternoon of 10 September. The average rainfall intensity was 45 mm per day. During both rainfall periods, in the morning of each day, the artificial rainfall was stopped for two or three hours to allow the measurement of horizontal displacements and soil swelling, as well as to auger disturbed specimens for the determination of gravimetric water content profiles. Apart from this regular stoppage, the artificial rainfall intensity was maintained at a constant rate of 2.9 mm/hr. During the artificial rainfall period in the bare area, three short and heavy natural precipitations occurred. The total rainfall depth, including both artificial and natural rainfalls, in the bare area was about 430 mm.

Similar to the bare area, the grassed area also had experienced about seven months of drought before 1 June. However, from 1 June to 18 September when the artificial rainfall started, the grassed area was exposed to natural precipitation and evaporation.

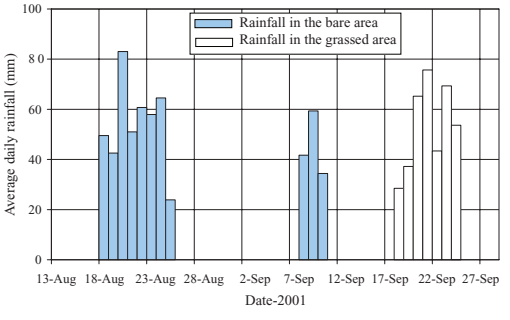

Figure 11. Artificial rainfall events simulated in both the bare and the grassed areas.

During this period, the total precipitation was about 250 mm. Consequently, the initial groundwater conditions in the grassed area were different from the relatively dry ground conditions in the bare area. Artificial rainfall events were produced in succession in the bare and the grassed areas. As shown in Figure 11, the simulated rainfall in the grassed area lasted about seven days from the morning of 18 September to the afternoon of 24 September. It should be noted that the intensity of the artificial rainfall in the grassed area was close to that in the bare area, i.e., 2.9 mm/hr. No natural precipitation was recorded during the artificial rainfall period in the grassed area. Thus, the total rainfall depth in the grassed area was about 380 mm. The average rainfall intensity was 53 mm per day, 9 mm less than that of the first rainfall event in the bare area. The rainfall pattern simulated in the grassed area was similar to the first rainfall event simulated in the bare area, with the exception of the slightly smaller daily rainfall intensity. In the grassed area, the rainfall was stopped to take soil samples every second day.

5 OBSERVED FIELD PERFORMANCE

In this section, the monitored results obtained from the bare area are presented first. The monitored results include surface runoff, soil suctions or pore-water pressures, water contents, horizontal stresses, horizontal displacements and soil swelling. Then, the performances of the bare and grassed areas are compared. The performances include surface runoff, pore-water pressures and water contents. Thereafter, the effects of vegetation on rainfall infiltration and slope stability in the unsaturated expansive soil are discussed based on the monitoring results.

5.1 *Field performance of the bare area (Ng et al. 2003)*

5.1.1 *Surface runoff*

The percentage of infiltration during the two rainfall periods is shown in Figure 12, along with the daily rainfall intensity. The percentage of infiltration is equal to the difference between the rainfall intensity and the surface runoff divided by the rainfall intensity. During the first one and a half days after the beginning of the first artificial rainfall event, the percentage of infiltration was essentially 100%, which means that no runoff was measured. Then, the percentage of infiltration decreased significantly with rainfall duration because of an increase in the runoff. After four days of rainfall, the percentage of infiltration reduced to about 35%, and the decreasing rate became much less significant. In other words, about 65% of the rain ran off after the first rainfall event had lasted for four days. The decrease in the percentage of infiltration was likely related to the closure of open cracks

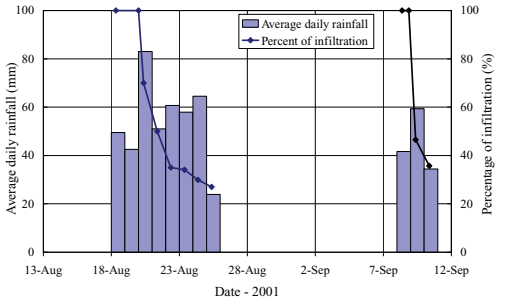

Figure 12. Percentage of infiltration during rainfall periods in the bare area (Zhan 2003).

and fissures due to swelling of the expansive soil upon wetting. In the second rainfall period, during the first 12 hours after the beginning of the rainfall, the percentage of infiltration was essentially 100% (i.e., no runoff). Thereafter, the percentage of infiltration decreased dramatically with rainfall duration. It reduced to 46% and 35% after one and two days, respectively. The prompt and dramatic decrease in the percentage of infiltration was probably caused by the initial wet ground conditions and the closing up of the initial cracks and fissures.

5.1.2 *Soil suction or pore-water pressure (PWP)*

Pore-water pressures or soil suctions in the bare area were measured by jet-filled tensiometers and thermal conductivity sensors. The tensiometers were used to measure negative pore-water pressure up to 90 kPa. However, they can also measure limited positive pore-water pressure because of the elevation head difference between the ceramic cup and the gauge. The measurement of soil suction by using a thermal conductivity sensor is an indirect method, and its working principle does not allow for the measurement of positive pore-water pressure. Therefore, the results measured by the tensiometers should be presented in terms of pore-water pressure (PWP), whereas the results measured by the thermal conductivity sensors should be presented in terms of soil suction. Since the changes of *in-situ* PWP or soil suction, in response to the simulated rainfalls, exhibited similar characteristics in the three different sections (i.e., R1, R2 and R3 located at the upper, middle and lower sections of the slope, respectively), typical results at R2 have been selected and shown in Figure 13. The results recorded by four tensiometers and four thermal conductivity sensors at R2 in the bare area are presented in terms of PWP and soil suction in Figures 13a and b, respectively.

As show in Figure 13a, the negative PWPs increased with time before the first rainfall. On 13 August, the negative PWPs ranged from 7 to 43 kPa. Immediately prior to the first artificial rainfall on 18 August,

negative PWPs ranging from 18 to 62 kPa were recorded. This indicated that the soil was under drying conditions before the first rainfall. As expected, the higher the elevation of the tensiometer, the larger the negative PWP. As shown in Figure 13b, with the exception of thermal conductivity sensor (R2-TC-0.6) showing a very high soil suction of about 250 kPa at 0.6 m below ground, soil suctions deduced from the remaining three sensors were generally consistent with the measurements obtained from the tensiometers.

During the first two days after the first artificial rainfall that began on 18 August, the negative PWPs at different depths all continued to increase slightly as shown in Figure 13a. The negative PWPs began to decrease after about two days of rainfall. In other words, there was a clear delay in the PWP response to rainfall infiltration, even at a depth of 0.6 m. Within the depth of 1.5 m, the duration of delay appeared to decrease as the depth increased. Based on field reconnaissance and observations in trial pits, it was found that many open cracks and fissures appeared near the ground surface. Besides, a relatively impermeable layer was identified at about 1.5 m below the ground surface. The presence of the impeding layer may be attributed to the lack of open cracks and fissures. Since intact expansive clay has a relatively low water permeability (on the order of 10^{-7} m/s), it is postulated that water can only make ingress into the clay through cracks and fissures. In the beginning of the first rainfall, rainwater flowed through the cracks and fissures, so the tensiometers did not register any significant changes of soil suction around their tips and this led to the initial response delay. Subsequently, when the infiltrated rainwater started to rise from the bottom of the cracks or from a perched water table formed due to the presence of the impeding layer and seep in all directions, the lower the tensiometer, the quicker the response (i.e., the shorter the delay). When water reached the locations of the tensiometers above the impeding layer, a rapid response was shown by the sharp reduction in negative PWP. The magnitude of reduction in negative PWP appeared to be governed by the depth of the measuring device. Tensiometers located at shallower depths recorded a larger reduction in negative PWP than those at deeper depths, due to the higher initial negative PWP present in the shallower depths. The magnitude of reduction in negative PWP at 0.6 m below ground was almost twice of that at 1.4 m depth. The tensiometer located below the impeding layer showed the slowest and the most gradual rate of response to rainfall and the lowest magnitude of reduction of negative PWP. After the rapid reduction in negative PWP, the top three tensiometers appeared to establish "final equilibrium" conditions within a day. All three tensiometers recorded positive PWPs ranging from 10 to 12 kPa. The PWP measured by the tensiometer located at 1.6 m depth was slightly lower than those measured by the top three.

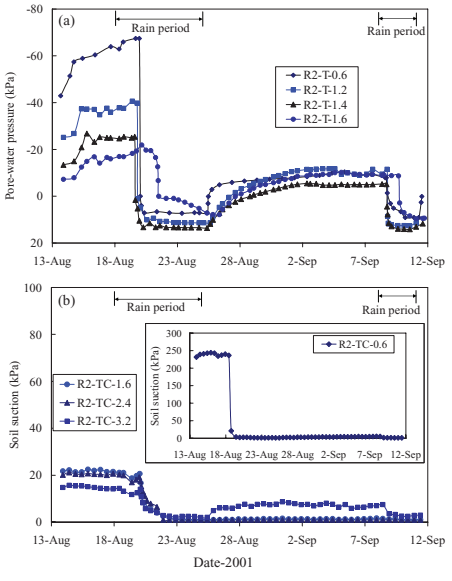

Figure 13. Response from suction sensors located at R2 in the bare area: (a) pore-water pressures measured by tensiometers, (b) soil suctions measured by thermal conductivity sensors (Ng et al. 2003).

After the first rainfall was completed, the lower three tensiometers showed a gradual increase (or recovery) in negative PWP and appeared to reach a steady state condition after 2 September. The rates of recovery were very similar to each other. On the other hand, the negative PWP measured by the top tensiometer showed a much more rapid initial recovery. However, the final magnitudes of all the four recovered negative PWPs fell within a narrow range (from 3 to 10 kPa) and did not appear to be strongly governed by the depths of the tensiometers.

Unlike the responses of tensiometers in the first rainfall, the lower three tensiometers showed almost no delay in response to the second rainfall. There was a change in PWP from negative to positive, although the magnitude of the change was not very significant, i.e., about 10 kPa. On the other hand, the top tensiometer showed a one-day delay in response to the second rainfall. However, the "final equilibrium" PWPs recorded during the second rainfall was similar to those during the first one.

Figure 13b shows the soil suction responses to the two artificial rainfalls measured by thermal conductivity sensors in the bare area. The responses were similar to those recorded by the tensiometers (see Fig. 13a), but the former showed a slower rate of response than the latter. The magnitudes of PWPs or suctions measured by the two different types of sensors were generally consistent, particularly at the depth of 1.6 m below

ground. However, the thermal conductivity sensor at 0.6 m below ground showed a very high soil suction of about 250 kPa before the first rainfall, which was much larger than the negative PWP of about 62 kPa measured by a tensiometer. This inconsistency between the results of the two sensors may be due to the inherent limitation of tensiometers caused by cavitation at high suction.

The *in-situ* PWP distributions with depth at R1, R2 and R3 are shown in Figures 14a, b and c, respectively. Before the commencement of the first rainfall period, the PWP profiles generally exhibited an increase in PWP with depth. The negative PWPs near the ground surface were substantially higher than those at greater depths, and hence the PWP profiles deviated significantly from theoretical hydrostatic conditions. The negative PWPs below a depth of 2 m were relatively low and they decreased gently with an increase in depth. A vertical upward seepage condition could be seen in all three sections. The negative PWPs within 2 m depth were highest and lowest at sections R1 and R3, respectively, dependent on the elevations of the sections.

After three days of heavy rainfall, the PWPs increased significantly within the upper 2 m of soil. A positive PWP appeared at a depth of about 1.5 m below the ground at all the three sections. The continued rainfall after 21 August resulted in a further

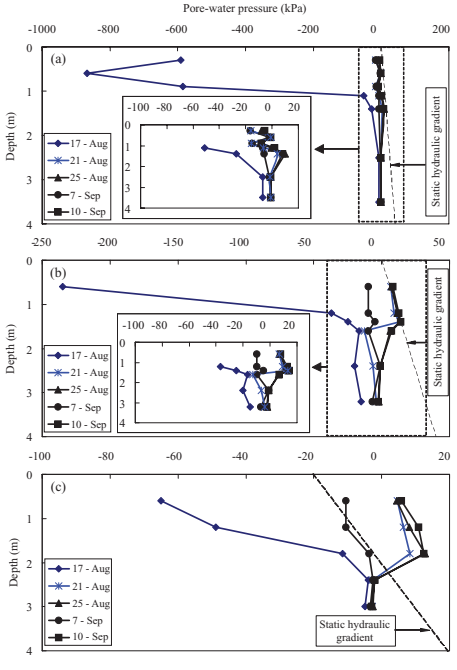

Figure 14. Variations in *in-situ* pore-water pressures with depth in the bare area: (a) at R1, (b) at R2, (c) at R3 (Ng et al. 2003).

increase in PWPs, but at a significantly reduced rate. At the end of the first rainfall period (i.e., 25 August), significant positive PWPs were observed by tensiometers within the upper 2 m of soil, with the largest at a depth of about 1.5 m at each section. This seemed to indicate the presence of a perched groundwater table at about 1.5 m below the ground surface. The measured *in-situ* dry density profiles demonstrated that there was a dense ($\rho_d \geq 1.60$ Mg/m^3) soil layer, ranging from 0.3 to 0.5 m, located at about 1.5 m. It is believed the dense soil layer possessed a relatively low coefficient of water permeability, and hence the infiltrated rainwater was retained above this dense layer. Due to the impedance effect of the dense layer, the influence of rainfall on PWP below the 1.5 m depth at this site was generally insignificant. The presence of the perched groundwater table at a depth of about 1.5 m caused the development of significant positive PWP, which led to the expansion of the initially dry expansive soil upon wetting, resulting in a reduction in the shear strength of the soil layer. This may explain why most rain-induced landslides appear to be relatively shallow, generally within a 2 m depth (Bao & Ng 2000).

Two weeks after the end of the first rainfall (i.e., on 7 September), a recovery of negative PWP was observed within a depth of 2 m at all three sections. The recovered negative PWPs were much smaller than the corresponding values before the commencement of the first rainfall, particularly near the ground surface. At the end of the second rainfall period (i.e., on 10 September), the PWP profiles were similar to those observed at the end of the first rainfall at all three sections.

5.1.3 *Water content*

Figure 15 shows the monitored results of volumetric water content (VWC) by four Theta-probes located at R2 during the two artificial rainfalls in the bare area. The response of VWC was generally consistent with the corresponding PWP response. Before the first rainfall, the measured VWCs increased with depth from 33% to 41%, suggesting that evaporation had taken place. After the commencement of the first rainfall, there was a delay in the response of VWC to rainfall, similar to the delayed response of PWP (see Fig. 13). With the exception of the Theta-probe located at 0.3 m below the ground surface (i.e., R2-θ-0.3), there was a delay of about two days in changes in VWC in response to the first artificial rainfall. The infiltration characteristics revealed by the lower three Theta-probes were generally consistent with the PWP responses. The one at 1.2 m depth (R2-θ-1.2) responded first, followed by the one at 0.6 m depth, and finally the one at 1.6 m depth. The order of response may perhaps be explained by the presence of an impeding layer located at about 1.5 m depth as discussed previously. The rapid

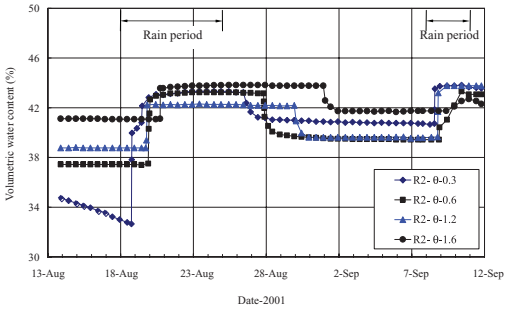

Figure 15. Volumetric water content changes in response to rainfall measured by the Thetaprobes located at R2 in the bare area (Ng et al. 2003).

response of R2-θ-0.3 might be attributed to the presence of a large number of cracks and fissures near the surface.

After three days of rainfall, all measured VWC at various depths appeared to reach a steady state condition, ranging from 42 to 44%. About three days after the cessation of rainfall, the VWC at different depths began to decrease progressively to another steady state condition, ranging from 40 to 42%. The shallower probes reached new equilibrium values first followed by the deeper ones. All the VWCs reached new equilibrium values by 2 September and remained unchanged until the second rainfall started on 8 September. After the start of the second rainfall, all the four Theta-probes responded quite rapidly, but the magnitude of the increase in VWC was generally smaller than that during the first rainfall.

Similar responses were observed from the Theta-probes installed at sections R1 and R3, except that there was a difference in the magnitude of VWC. The initial VWCs within 1 m of ground surface were lowest and highest at R1 and R3, respectively, dependent on the elevations of the sections. This is consistent with the responses of PWP.

The variations of *in-situ* water content profiles in response to rainfalls are shown in Figure 16. The solid lines marked with solid symbols or asterisk symbols represent the gravimetric water content (GWC) profiles obtained by direct sampling of the soil. The solid lines labelled with open symbols represent the volumetric water content (VWC) profiles measured by Theta-probes. The two dashed lines in the middle of each figure are the calculated lower and upper bands of the VWC profiles calculated from the measured GWC profiles and the measured dry density profiles.

Just prior to the commencement of the first rainfall event (i.e., on 17 August), the measured initial GWCs near the ground surface ranged from 16 to 20% at different sections. The initial GWCs at three sections all increased with depth within 1.5 m below ground, suggesting an upward flow of moisture via evaporation. The measured relationships between initial GWC profiles and the measured initial negative PWP profiles are shown in Figure 8, along with the SWCCs measured in the laboratory. As discussed previously, the *in-situ* relationships between GWC and soil suction were approximately consistent with the wetting curve of the SWCC.

The variations in the measured GWC profiles were generally consistent with those of the PWP responses. As shown in Figure 16, after the start of the first rainfall, a significant increase in GWC was observed within the upper 1.5 m below ground. However, the influence of the rainfall on the GWCs below 1.5 m seemed to be essentially negligible, particularly at R2. This finding supports the previous postulation that there is a low permeability layer at 1.5 m depth. During the two-week no-rain period after the end of the first rainfall, all the GWCs decreased. However, the reduction appeared to be small, even in the soil layer near the ground surface. At the end of the second rainfall (i.e., 10 September), the GWCs increased to values close to those at the end of the first rainfall (i.e., 25 August).

It can be seen in the figure that the VWCs measured by Theta-probes are generally significantly larger than the upper bound of the VWC calculated from the

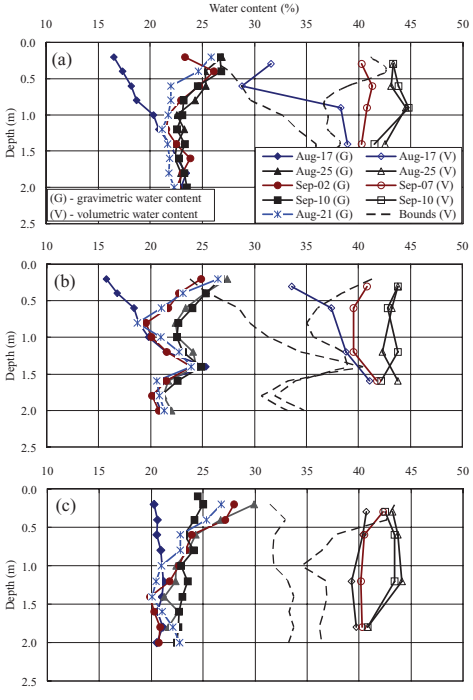

Figure 16. Variations in water contents in relation to depth in the bare area: (a) at R1, (b) at R2, (c) at R3 (Ng et al. 2003).

GWC and dry density profiles in all three sections. The inconsistency between the measured and calculated VWCs may be attributed to the inaccuracy of the indirect measurements of VWC using Theta-probes. The measuring accuracy using Theta-probes can be affected by many factors such as the variations in soil composition, dry density and cracks (Thetaprobe 1999, Li et al. 2002). It is suggested that the measured VWC can only be interpreted as an indication of what is happening.

5.1.4 *Horizontal total stress*

The horizontal total stresses (σ_h) were measured by six vibrating-wire earth pressure cells (EP1-6 in Fig. 9) installed in the bare area. All six earth pressure cells were installed at a depth of 1.2 m, giving rise to an estimated total vertical stress (σ_v) of about 23.4 kPa, which corresponded to an average dry density of 1.56 Mg/m^3. Figure 17 shows the variations in the monitored total stress ratio (σ_h/σ_v) in relation to time from the six earth pressure cells in the bare area. Pressure cells EP1, EP3 and EP5 measured the stress changes acting in the East-West (EW) direction (i.e., perpendicular to the inclination of the slope), whereas EP2, EP4 and EP6 recorded pressures acting in the North-South (NS) direction (i.e., parallel to the inclination of the slope).

Prior to the first rainfall, the total stress ratios recorded by all the pressure cells were lower than 0.3. An initial equilibrium stress ratio appeared to have been established for each pressure cell shortly before the start of the rainfall. Two out of the six pressure cells registered a small tensile stress, probably induced as a result of soil drying. After the start of the first rainfall, all earth pressure cells did not register any significant changes of stress for about one and a half days. The delayed response of the earth pressure cells was consistent with the PWP and VWC responses. Once the earth pressure cells started to respond, the stress ratios increased rapidly and significantly within one day and then approached a steady value during the first rainfall event. The magnitude of increase in total horizontal

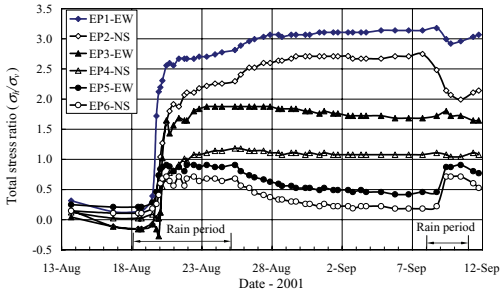

Figure 17. Variations in *in-situ* total stress ratios measured by earth pressure cells in the bare area (Ng et al. 2003).

stress was strongly related to the elevation of the earth pressure cells and the initial negative PWP. When the elevation of the earth pressure cell was higher, the initial negative PWP present in the ground was larger, and hence the increase in σ_h/σ_v was larger. The measured σ_h/σ_v by EP1 and EP2 increased to 2.8 and 2.3, respectively. However, the measured σ_h/σ_v by EP5 and EP6 only increased to 0.9 and 0.7, respectively. For a given pair of pressure cells located at the same elevation, the measured stress ratio in the EW direction was always larger than that in the NS direction. This is probably related to a higher constraint imposed as a result of the sloping ground in the EW direction as opposed to that in the NS direction.

After the end of the first rainfall, a further increase in σ_h/σ_v was observed at EP1 and EP2 during the two-week no-rain period. The continuous and gradual increase in σ_h/σ_v at EP1 and EP2 (but at a reduced rate) might be due to an ongoing "soaking" of the soil near the location of the earth pressure cells at R2, even after the first rainfall event. On the other hand, the EP3 and EP4 pressure cells showed a slight decrease in σ_h/σ_v throughout the no-rain period, and EP5 and EP6 recorded a larger reduction in σ_h/σ_v. The reduction in σ_h/σ_v may be primarily due to a decrease in the positive PWP at a depth of 1.2 m during the no-rain period.

After the start of the second rainfall event, the responses of the three pairs of earth pressure cells were distinctly different. At EP1 and EP2, the observed σ_h/σ_v decreased rather then increased. This may be attributed to the softening of the soil after prolonged swelling during the no-rain period. In the earth pressure cells near the toe of the slope (EP5 and EP6), an increase in σ_h/σ_v was recorded due to the positive PWP during the second rainfall. The performance of EP3 and EP4 fell between the former two cases.

In order to compare the measured total stress ratios after the simulated rainfalls and the corresponding theoretical limiting conditions, the total stress ratios at the passive failure conditions were calculated using the "total stress" and "effective stress" approaches (Fredlund & Rahardjo 1993). In the "total stress" approach, the undrained shear strength was assumed to be equal to 4.4 times the SPT N value obtained in the monitored area after the rainfall. The calculated total stress ratio for passive earth failure conditions was 4.4, which was greater than the measured earth pressures except those at EP1 and EP2, which appeared to be close to passive failure conditions. In the "effective stress" approach, the calculated total passive stress ratio ranged from 2.0 to 3.1, if the saturated shear strength parameters, $c' = 5$ to 15 kPa and $\phi' = 17°$ obtained from testing specimens with fissures and cracks (Liu 1997) were used in the calculations. The calculated passive stress ratios were close to the measured values recorded by EP1 and EP2 after the simulated rainfalls. This seemed to suggest that

the expansive soils after the simulated rainfalls may reach passive failure along existing cracks and fissures. This finding is consistent with that observed by Brackley & Sanders (1992). This further supports the observation of possible softening behaviour in the soil upon prolonged wetting. The high *in-situ* stress ratio due to the swelling of expansive soils upon wetting might be one of the main reasons for the retrogressive shallow failures found near the monitored slope.

5.1.5 *Ground deformations*

Figure 18 shows horizontal displacements profiles of the ground in response to the simulated rainfalls in the bare area. Horizontal displacements of the ground were calculated from the tilting measured by the inclinometers. The rotations measured just prior to the commencement of the first rainfall were taken as the reference datum. The calculated displacements of the inclinometers from the South to the North direction and from the West to the East direction were defined as positive.

Figures 18a and b show the monitored horizontal displacements from inclinometer I1 located just above the mid-slope in the NS and EW directions, respectively. The results indicate that the ground moves toward the down-slope direction and towards the East direction. The measured horizontal displacements in the two directions show similar characteristics. The horizontal displacements in the upper 1.5 m were understandably more significant than those below this depth, which looked like a "cantilever" mode of deformation. The variations in horizontal displacement profiles were consistent with the changes of PWP and water content, which showed that the most significant changes took place at shallow depth (i.e., less than 1.5 m).

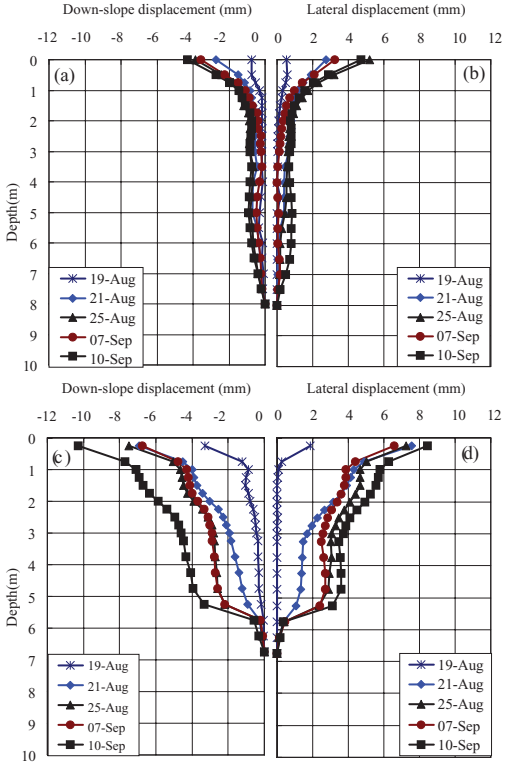

Figure 18. Observed horizontal displacement in response to rainfalls in the bare area: (a) from I1 (NS), (b) from I1 (EW), (c) from I2 (NS), (d) from I2 (EW) (Ng et al. 2003).

The horizontal displacements measured on 19 August (after one day of rainfall) were small (less than 1 mm) in both directions, probably because of the delayed response similar to PWP. After three days of rainfall (i.e., on 21 August), there was a significant increase in horizontal displacements in both directions, particularly near the ground surface where both displacements increased to about 3 mm. As the rainfall continued, further changes in the horizontal displacement were relatively insignificant. After the first rainfall event, a recovery of horizontal displacement (i.e., a shrinkage response) was observed with respect to both directions during the two-week no-rainfall period, due to the increase in soil suction or decrease in positive PWP. The recovery of horizontal displacement from the East to the West direction was about 2 mm, which was almost 10 times of that in the up-slope direction (i.e., only about 0.2 mm). This may be because the effects of an increase in soil suction on the up-slope movements were counteracted by the influence of gravity in the inclination direction of the slope. At the end of the second rainfall event, the observed horizontal displacements were similar to those measured at the end of the first rainfall in both directions. This was consistent with the PWP and GWC responses.

Figures 18c and d show the monitored horizontal displacements from inclinometer I2 located near the toe of the slope in the NS and EW directions, respectively. It can be seen that the magnitudes of displacement and deformed shapes observed in both directions were fairly consistent. Similar to the variations in horizontal displacements at I1, the horizontal displacements increased significantly due to rainfalls, particularly near the ground surface where the increases were about 4 and 6 mm in the NS and EW directions, respectively. After the first rainfall, the changes in horizontal displacements were relatively small during the two-week no-rainfall period.

It should be noted that the magnitudes of displacements at I2 were significantly larger than those at I1. The final displacements at I2 were 2 to 2.5 times of those at I1. The depth of influence at I2 was about 6 m, more than 3 times of that at I1 (less than 2 m). These may be because the initial soil suction at I2 was lower

than that at I1, resulting in smaller soil stiffness at I2. This is probably one of the main reasons for the retrogressive shallow failures found near the monitored slope. The greater influence depth at I2 was consistent with the deeper influence of the simulated rainfalls on the GWC measured at section R3, as opposed to section R2.

At both I1 and I2, the consistently observed eastern movements of the ground due to rainfall infiltration might be attributed to the direction of the sub-surface water flow from the West to the East caused by the presence of slightly dipping geological planes. On 23 August, a seepage exit point was observed at about 15 m to the East along the lower part of the masonry wall, outside the bare area. This observation seemed to support the postulation on the direction of water flow and ground movement.

Figures 19a, b and c show the measured vertical swellings of the ground in response to the simulated rainfalls near the three sections, R1, R2 and R3, respectively. It can be seen from Figure 19a that there are two movement points located at a depth of 0.1 m, one at 0.5 m and one at 1.0 m depth near R1. One day after the commencement of the first rainfall event, one of the top two movement points registered an upward soil movement of about 6 mm, while the other one did not record any significant movement. Then the upward movements of the top two movement points increased at an almost constant rate during the following four days of rainfall. Thereafter, the soil continued to swell but at a reduced rate, throughout the remainder of the monitoring period. On the other hand, there was no recorded swelling at the movement points embedded at both 0.5 m and 1.0 m depths during the first four days of rainfall. Then, the soil at the two depths started to swell at a rate similar to that recorded at the depth of 0.1 m. As anticipated, the movement point embedded at shallower depth recorded a larger magnitude of swelling. This was likely due to the larger changes in the soil suction at shallower depth associated with rainfall infiltration and the accumulative swelling of all the soil beneath them.

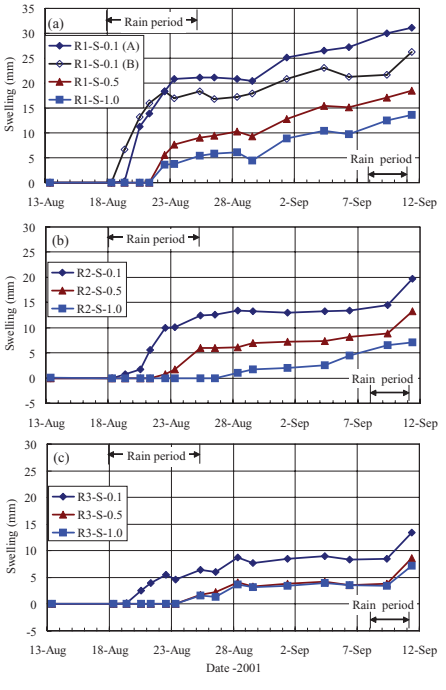

Figure 19. Soil swelling at shallow depths: (a) near R1; (b) near R2; (c) near R3 (Ng et al. 2003).

At the end of the rainfall event, the soil swelling at R1 ranged from 5 to 21 mm at different depths. During the two-week no-rain period, the ground continued to swell but at a reduced rate. The continuous soil swelling at all three depths could be attributed to the slow seepage of infiltrated water from open cracks and fissures into the surrounding soil, leading to the secondary swelling of the expansive soil. Marked secondary swelling behaviour has been observed and reported by Chu & Mou (1973) and Sivapullaiah et al. (1996). Alonso (1998) postulated that marked secondary swelling behaviour of expansive clays is due to the slow and progressive hydration of the expansive soil's microstructures. During the second rainfall event, the rates of soil swelling increased, particularly at the depth of 0.1 m.

The observed soil swelling patterns near R2 and R3 were similar to those observed near R1, as shown in Figures 19b and c. However, the durations of the delayed responses to rainfalls were longer. Since one of the movement points at 0.1 m depth was broken, only one movement point at 0.1 m depth was recorded. At a given depth, the magnitudes of soil swelling near R2 and R3 were smaller than that observed near R1. The maximum swelling near R1, R2 and R3 were about 31, 20 and 13 mm, respectively. This is probably due to the smaller initial soil suctions at R2 and R3. Based on the measurements at the three sections, a generalization that the higher the initial suction, the larger the soil swelling at a given depth can be made. Within the same section, the shallower the embedded movement point, the larger the measured soil swelling.

5.2 *Comparisons of performance between the bare and grassed areas (Ng & Zhan 2007)*

The performances of the bare and grassed areas are compared in this section. Only the responses of the bare area to the first simulated rainfall are considered for comparison purposes. As shown in Figure 11, both areas were subjected to seven days of artificial rainfall.

5.2.1 *Surface runoff*

Figure 20 shows a comparison of infiltration rates between the bare and the grassed areas. The duration of rainfall in the figure is calculated by taking the starting time of the simulated rainfall as a reference point, i.e., 18 August in the bare area and 18 September in the grassed area. The infiltration rate is assumed to be equal to the difference between the measured rainfall intensity and the surface runoff. It is recognized that this calculation is not strict for the grassed area, since the grass cover may intercept and adsorb some rainfall. However, Branson et al. (1972) estimated that the storage capacity of grass ranges from 1 to 5 mm of rainfall, which is only a very small portion as compared with the simulated rainfall in the grassed area (380 mm in total). Hence, the deduced infiltration rate is accurate enough.

The intensity of the artificial rainfall simulated in the two areas was very close, about 2.9 mm/hr. Just after the commencement of the rainfall, the infiltration rate was equal to the rainfall intensity, because no surface runoff was measured. In the bare area, the infiltration rate started to decrease dramatically with the duration of rainfall after one and a half days of rainfall, as indicated by the onset of surface runoff. On the other hand, in the grassed area, the infiltration rate started to decrease after about three days of rainfall. This means that the surface runoff in the grassed area had a longer delay. During the one-week rainfall, the infiltration rate in the grassed area was equal to or greater than that in the bare area. At the end of the rainfall, the infiltration rate at equilibrium in the grassed area was about 0.8 mm/hr greater than that in the bare area (i.e., more than twice the amount). This means that more rainwater infiltrated into the soil in the grassed area. The observed differences in infiltration rates may be primarily attributed to the effects of vegetation. A detailed explanation is given in section 5.3. Besides, the different soil moisture conditions prior to the simulated rainfall may also have contributed to the observed infiltration difference between the two areas. This will be discussed in section 5.2.2.

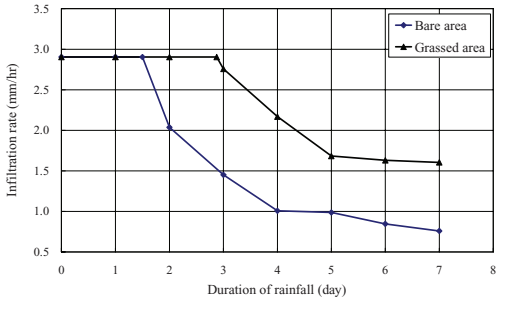

Figure 20. Comparison of infiltration rates between the bare and grassed areas (Ng & Zhan 2007).

5.2.2 *Soil suction or pore-water pressure (PWP)*

Figures 21a, b and c show a comparison of pore-water pressure (PWP) responses to the simulated rainfall between the bare and grassed areas at sections R1, R2 and R3, respectively. At each section in each area, two PWP response curves measured near 1.2 m and 1.6 m were selected for comparison. All the PWPs in the figure were measured by jet-filled tensiometers. Just after the commencement of the rainfall, negative PWPs were measured in both areas. The values measured in the grassed area were larger than those measured in the bare area, particularly near the depth of 1.6 m where the negative PWPs in the grassed area were 2 to 3 times of those in the bare area. The negative PWPs showed a delay of 1.5 to 2 days in the bare area, with the exception of tensiometer (R2-T-1.6). The negative PWPs recorded in the grassed area showed a longer duration of delay, about 2.5 to 3 days. The duration of delay in the PWP response was generally consistent with the onset of surface runoff in both areas. After the onset of PWP response, the increase of PWP with the duration of rainfall in the grassed area was found to be more gradual than that in

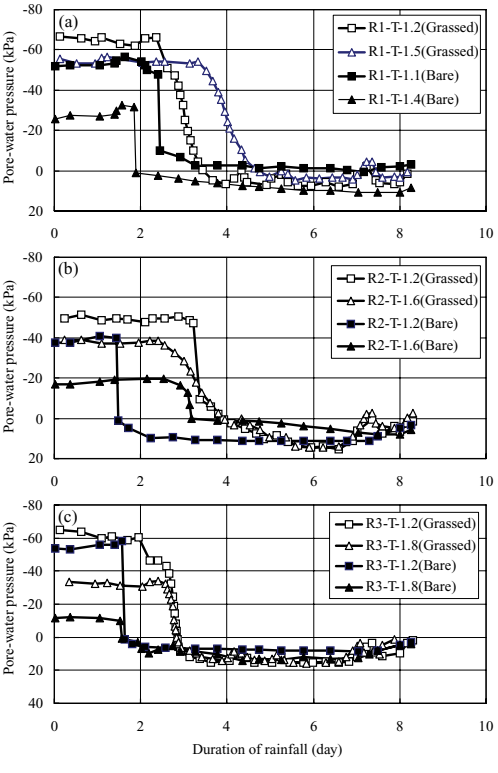

Figure 21. Comparison of pore-water pressure responses from tensiometers in the bare and grassed areas: (a) at R1, (b) at R2, (c) at R3 (Ng & Zhan 2007).

the bare area, especially at the upper part of the slope (i.e., at R1). This will be explained later. At the end of the simulated rainfall, positive PWPs were recorded in both areas, and the values of PWP for a given depth were close to each other in the two areas.

Figures 22a, b and c show a comparison of *in-situ* PWP profiles between the bare and grassed areas at sections R1, R2 and R3, respectively. In both areas, the initial PWP profiles just prior to the simulated rainfall, and those after one-week of rainfall, were selected for comparison. At shallow depths, such as the depths within 1 m below ground, the soil suction may exceed the measuring range of the tensiometers. Therefore, in the bare area, thermal conductivity suction sensors were used to measure the soil suction near the ground surface. In the grassed area, only data blow a depth of 0.9 m are presented, because no measurements of PWP were taken in the shallower soil layer.

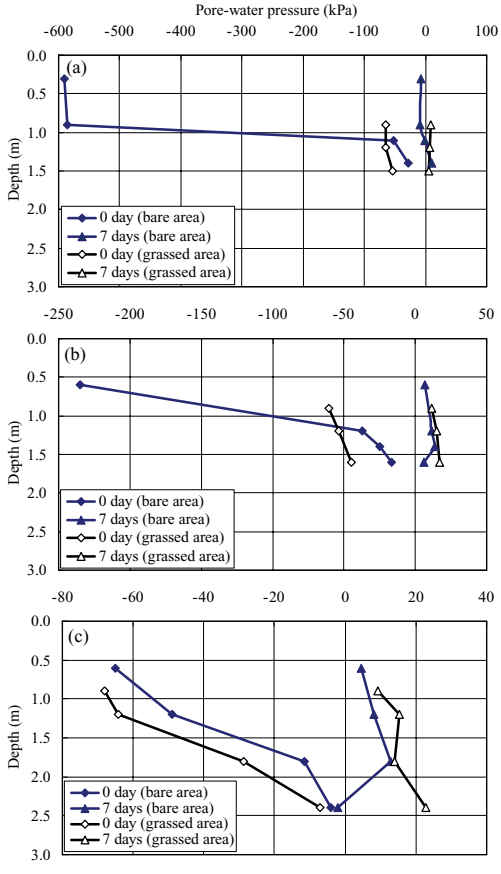

Figure 22. Comparison of *in-situ* pore-water pressure profiles in the bare and grassed areas: (a) at R1, (b) at R2, (c) at R3 (Ng & Zhan 2007).

Just prior to the simulated rainfall, the negative PWPs within the top 1 m in the bare area were significantly higher than those in the grassed area at both sections R1 and R2. As explained by Ng et al. (2003), the high soil suctions within the top 1 m in the bare area, at the upper part of the slope in particular, appear to be related to the excessive evaporation enhanced by the wide-open cracks near the ground surface. The measured daily evaporation potential from the free water surface prior to the simulated rainfall ranged from 3 to 10 mm. Another reason for the higher soil suction within the top 1 m depth in the bare area may be due to the difference in the initial groundwater conditions prior to the rainfall. From 1 June to 18 August before the simulated rainfall, the bare area was protected by a plastic membrane from rainfall infiltration. However, the grassed area was exposed to natural precipitation from 1 June to 18 September, during which the total precipitation was about 250 mm. The higher soil suction in the bare area would tend to result in a lower coefficient of water permeability but a higher hydraulic gradient in the upper soil layer, which may have contributed to the observed difference in the infiltration rate between the two areas (see Fig. 20).

The case for the soil layer below 1 m depth followed an opposite trend to that explained above, as shown in Figure 21. The initial soil suctions in the grassed area were higher than those in the bare area below 1 m depth. This behaviour may be attributable to the transpiration effect of the grass cover. The growth of plants extracts water from the soil. The transpiration of plants requires an increased demand for water and hence it can result in more significant soil moisture depletion in the ground (Holtz 1983, Hillel 1998). The soil moisture depletion in turn leads to an increase in soil suction in the soil near the root system as well as in the zone beyond the root system, i.e., the influence zone (Driscoll 1983, Richard et al. 1983). The average height of the grass (H) on the slope surface was about 0.5 m. By using the calculation method by Ward (1953) and Richard et al. (1983), the transpiration impact of the grass in the grassed area may affect the soil suction in the soil layer as deep as 1.2 m or more. The above discussion may help to explain the higher soil suction below a depth of 1 m in the grassed area as opposed to that in the bare area. As discussed before, the 250 mm of natural rainfall on the grassed area may also have contributed to the difference in soil suction between the two areas. However, the influence of natural rainfall might only be significant near the ground surface since the rainfall amounting to 250 mm was scattered over a three-month summer period and the advancement of the wetting front could be reduced by the evapotranspiration in the grassed area (Lim et al. 1996). Because of the evapotranspiration effect, the soil suction within the root zone in the grassed area might also be higher than the corresponding soil suction in

the bare area. It is unfortunate that no measurements of soil suction were taken in the shallow soil layer in the grassed area.

At the lower part of the slope as shown in Figure 22c, the initial negative PWPs measured in the grassed area appear to be higher than those in the bare area at all the depths within the top 2.5 m. The higher negative PWPs may be attributable to the predominant evapotranspiration effect of the grass in the grassed area over the evaporation in the bare area. The above data were consistent with the field observation in a residual soil slope made by Lim et al. (1996). They found that the presence of vegetation could significantly increase *in-situ* matric suction. The deep influence of the grass observed above also supports the statement made by Coppin & Richards (1990). They pointed out that the ability of vegetation to modify soil suction was extensive and could reach beyond the physical extent of the roots.

The higher initial suction observed at a depth greater than 1 m in the grassed area at all the three sections, suggested that the depth of the open cracks in the grassed area was likely to be greater than that in the bare area. This is because the depth of the open cracks depends on the soil suction profile presented in the ground (Fredlund & Rahardjo 1993). The higher the soil suction, the greater the extent of shrinking to form cracks, which can propagate to greater depths of the soil layer. On the basis of linear elastic fracture mechanics, Morris et al. (1994) deduced that the depth of cracking was proportional to the depth of the groundwater level and soil suction was assumed to decrease linearly below the ground surface. As an intact expansive clay generally has a distinctly low water permeability, rainwater first infiltrates into the deeper soil layer through the open cracks and then rises from the bottom of the cracks and flows in all directions. Hence, those tensiometers installed at relatively shallow depths tended to show a longer delay in response to the rainfall. This may explain why the PWP responses measured in the grassed area showed a longer delay than that those observed in the bare area.

After one week of rainfall, the PWP profiles at section R1 in the grassed area did not differ significantly from the corresponding profiles in the bare area. At sections R2 and R3, the recorded positive PWPs in the grassed area were higher than those in the bare area, particularly at 1.6 m depth in section R2 and 2.5 m depth in section R3. The higher positive PWP was likely related to the presence of more significant perched groundwater below the grassed ground surface. At the end of the simulated rainfall, excessive free water was noticed at a depth of 2.5 m in the grassed area when samples were taken with an auger at the lower part of the grassed slope. However, the perched water table deduced from the bare area was at a depth of about 1.5 m, which was 40% shallower than that observed in the grassed area.

5.2.3 *Gravimetric Water Content (GWC)*

Figure 23 shows a comparison of gravimetric water content (GWC) profiles between the bare and grassed areas. The GWC profiles were obtained from direct sampling with an auger. In the figure, the GWC profiles just prior to the simulated rainfall and those after one week of rainfall were selected for comparison. The variation pattern of the GWC profiles in the grassed area was similar to that in the bare area. The GWC increased significantly after one week of rainfall in both the bare and grassed areas, especially at shallow depths. The maximum increase in GWC was about 10 kPa near ground. However, the depth of influence of the rainfall on the GWC profiles was greater in the grassed area than that in the bare area, particularly at R1. As shown in Figure 23a, the depths of influence at R1 in the bare and grassed area were about 1.5 m and 3.5 m, respectively. The GWC profiles at R2 and R3 are shown in Figures 23b and c, respectively. The depth of influence in the bare area appeared to be on

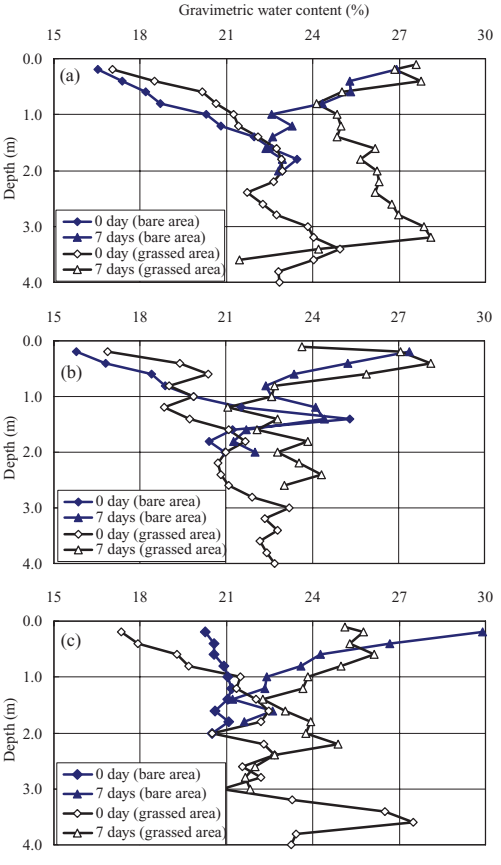

Figure 23. Comparison of water content profiles in the bare and grassed areas: (a) at R1, (b) at R2, (c) at R3 (Ng & Zhan 2007).

the order of 1.5 to 2 m, while the depth of influence in the grassed area was estimated to be about 2.8 m from the auger drilling records. In the grassed area, the increases in GWC below 1.5 m at R2 and R3 seemed to be not as significant as the increase observed at R1. It should be noted that the GWC profiles below 2.5 m were not obtained at the end of the rainfall since accumulation of water was observed in the sampling hole.

The greater depth of influence on GWC was consistent with the deeper perched groundwater observed in the grassed area as compared with that in the bare area. Besides, the difference in the depth of influence was consistent with the difference in the infiltration rate between the two areas. The greater depth of influence observed in the grassed area may be attributed to the greater depth of the open cracks and fissures. The deeper cracks tended to lead rainwater into the relatively deep soil layer and hence resulted in an increase in PWP and GWC in the soil.

5.3 *Effects of vegetation on rainfall infiltration and slope stability (Ng & Zhan 2007)*

The comparison of the results between the bare and grassed areas indicated that the vegetation in the grassed area exerted significant influences on the rainfall infiltration, which may in turn affect the slope stability.

In the bare area, the beating action of raindrops tends to result in a spontaneous slaking and breakdown of soil aggregates upon wetting (Bridge & Collis-Feorge 1973, Morel-Seytoux 1983). As a result, a thin less-permeable "crust" may form over the bare soil surface. Once formed, the surface crust can greatly impede water intake by the soil. On the other hand, the slackened soil particles can easily be detached and transported in the down-slope direction by the surface runoff, i.e., hydraulic erosion. During transport, some soil particles are moved into the open cracks on the surface and gradually fill the gaps. This may also result in a decrease in the infiltrability of the upper soil layer. These postulations were somewhat verified by examining the ground surface after the simulated rainfall events. After the rainfall, the slope surface in the bare area appeared to be more uniform than the initial ground surface that consisted of soil aggregates networked with a number of open cracks.

The vegetation in the grassed area may greatly change the surface water condition and infiltration. First, the grass cover may intercept and absorb a small proportion of the incoming rainfall. Second, the grass cover protects the soil on the ground surface from being struck directly and hence minimizes the formation of a less permeable crust on the slope surface (Hillel 1998). Third, the grass on the surface of the slope can increase surface roughness. On the other hand, the root systems of grass in the grassed area can provide more channels for water infiltration. In addition, the root systems of grass in the soil have a reinforcing effect, which may help to stabilize the soil aggregates, so that the relatively large inter-aggregate pores are maintained during rainfall. It is also postulated that the reinforcing effect may hinder the swelling of an expansive soil upon wetting and hence delay the closing of the open cracks and fissures. All the aspects described above may increase the permeability and infiltrability of the upper soil layer. Therefore, the grassed area showed a much greater infiltrability than the bare area did. As a result of a combination of greater infiltrability, rougher slope surface and interception of the grass cover, the onset of surface runoff in the grassed area was delayed longer than in the bare area. Hence, the responses of suction and water content also showed a longer delay in the grassed area.

The hydrological influences of grass on slope stability can be beneficial or adverse. During dry periods, grass has an evapotranspiration effect that can result in higher soil suction in both the root zone and the influence zone beyond the root systems, as compared to ground with a bare surface. This is beneficial to slope stability. However, the higher soil suction may in turn enhance the development of cracks in unsaturated expansive soils, resulting in a higher infiltrability during rainfall. On the other hand, grass can increase the infiltrability of the upper soil layer by providing more channels, preventing surface crusting, increasing surface roughness and delaying the closure of open cracks. All these influences of grass on rainfall infiltration are adverse to slope stability. However, the moisture loss via evapotranspiration and water absorption by the grass during rainfall was negligible compared with the applied rainfall intensity. Hence, the overall hydrological influence of grass on slope stability appeared to be adverse in this field study.

The simulated rainfall in the grassed area resulted in a more significant perched groundwater table and a greater depth of influence on pore-water pressures and water content. However, the real rainfall pattern in the field is generally different from the heavy and concentrated rainfall simulated in this field study, even during wet seasons. The real rainfalls during wet seasons are generally scattered over the period, and hence the influence of each rainfall on the grassed ground could be reduced or even counteracted by the evapotranspiration effect of grass during the subsequent no-rain period.

Therefore, it is difficult to draw a conclusion on the overall hydrological influence of grass on slope stability. A difficulty also lies in the quantification of the evapotranspiration effect of grass, which depends both on weather conditions and soil moisture deficits in the upper soil. However, it should be pointed out that the mechanical influences of vegetation on slope stability, such as root reinforcement, anchoring, arching and

buttressing effects of roots, are mostly beneficial to slope stability (Coppin & Richards 1990, Gray 1995).

6 CONCLUSIONS

The 1,427 km long canal of the middle-route of the SNWTP is expected to be a trapezoidal cross-section formed by cut and fill slopes. The potential instability of these slopes passing through 340 km unsaturated expansive soil zones imposes a major geotechnical challenge to the design and construction of the middle-route. A typical unsaturated expansive soil cut slope was therefore selected for a comprehensive and well-instrumented field study. Some key responses of the soil slope due to changes in both suction and net stress state, with and without vegetation, are summarized and discussed in this paper.

The observed responses in surface runoff, PWP, water content, horizontal stress and soil deformation in the bare area generally showed a one- to two-day delay related to the initiation of rainfall. The effects of the first three days of rainfall on the observed responses were much more significant than the effects of the ongoing rainfall and the second rainfall, probably due to the closure of open cracks.

The effects of the simulated rainfalls on slope performance were generally much more significant within 2 m of the ground surface. This may be explained by the presence of a relatively impermeable layer at about 1.5 m depth below ground. A significant perched water table was deduced at the depth of about 1.5 m due to the presence of the relatively impermeable layer. The presence of the perched ground water caused the development of significant positive PWP and an expansion of the initially dry expansive soil upon wetting. This led to a reduction in the shear strength of the soil layer. This may help to explain why most of rain-induced landslides occurring in similar unsaturated expansive soil slopes appear to be relatively shallow.

A significant increase in the total stress ratio (σ_h/σ_v) (up to 3) was observed after the simulated rainfalls, indicating the possibility of passive pressure failures in the softened clay. The high *in-situ* stress ratios due to the swelling of expansive soils upon wetting may be one of the main reasons for the retrogressive shallow failures found near the monitored slope.

Horizontal displacements of the ground were observed towards the down-slope after rainfall in the bare area. The magnitudes of displacements were significantly larger and the depth of influence was substantially deeper at the toe of the slope than those observed at the mid-slope. The final displacements measured at the toe were 2 to 2.5 times of those measured at the mid-slope. The depth of influence at the toe was more than 3 times of that at the mid-slope. These indicated the possibility of retrogressive slope failures.

Substantial soil swelling in the vertical direction was measured after the simulated rainfall, ranging from 7 to 31 mm at different depths and locations. The higher the initial soil suction, the larger the soil swelling. The observed vertical movement of the soil also revealed a marked secondary swelling characteristic of the expansive clay.

It was found that the variation patterns of surface runoff, PWP and GWC in the bare and grassed areas were similar, but the magnitudes were different. The duration of delay in the grassed area was about three days, which were longer than that observed in the bare area (i.e., one to two days). The depth of influence of the rainfall on the GWC profiles in the grassed area was about twice of that in the bare area. The greater depth of influence observed in the grassed area may be attributable to the greater depth of the open cracks. Besides, the perched groundwater deduced from the grassed area was about 2.5 m, 67% deeper and more significant than that in the bare area. At the end of the rainfall, the infiltration rate at equilibrium in the grassed area was more than twice the amount recorded in the bare area. All these results indicated that vegetation exerts significant influences on rainfall infiltration and slope stability.

ACKNOWLEDGEMENTS

The authors would like to acknowledge financial support from research grants HKUST6108/99E and HKUST6087/00E and in-kind support provided by the Yangtze River Scientific Research Institute, Wuhan China. The authors would also like to thank Professors C.G. Bao and D.G. Fredlund and Mr. B.W. Gong for their contributions to the field tests.

REFERENCES

Affendi, A.A. & Faisal, A. 1994. Field measurement of soil suction. *In Proceeding of 13th International Conference on Soil Mechanical and Foundation Engineering*, New Delhi, India: 1013–1016.

Alonso, E.E. 1998. Modeling expansive soil behavior. *2nd Int. Conf. on Unsaturated Soils*, Beijing, China. Vol. 2: 37–70.

Bao, C.G. & Ng. C.W.W. 2000. Keynote lecture: Some thoughts and studies on the prediction of slope stability in expansive soils. *1st Asian Conf. on Unsaturated Soils*, Singapore: 15–31.

Brackley, I.J.A. & Sanders, P.J. 1992. In situ measurement of total natural horizontal stresses in an expansive clay. *Géotechnique* 42(2): 443–451.

Branson, F.A., Gifford, G.F. & Owen, J.R. 1972. *Rangeland hydrology*. Society for Range Management, Range Science Series, No. 1.

Bridge, B.J. & Collis-Feorge, N. 1973. An experimental study of vertical infiltration into a structurally unstable swelling

soil with particular reference to the infiltration throttle. *Australia Journal of Soil Research* 11: 121–132.

Chu, T.Y. & Mou, C.H. 1973. Volume change characteristic of expansive soils determined by controlled suction tests. *3rd Int. Conf. on Expansive Soils*, Haifa: 177–185.

Coppin, N.J. & Richards, I. 1990. *Use of vegetation in civil engineering.* Butterwroths: Sevenoaks, Kent.

Driscoll, R. 1983. The influence of vegetation on the swelling and shrinkage of clay soils in Britain. *Géotechnique* 33(2): 93–105.

Favre, F., Boivin, P. & Wopereis, M.C.S. 1997. Water movement and soil swelling in a dry, cracked vertisol. *Geoderma* 78: 113–123.

Fredlund, D.G. & Rahardjo, H. 1993. *Soil Mechanics for Unsaturated Soils*. Wiley Interscience, New York.

Fredlund, D.G., Shui, F. & Feng, M. 2000. Use of a new thermal conductivity sensor for laboratory suction measurement. *1st Asian Conf. on Unsaturated Soils*, Singapore: 275–280.

Gray, D.H. 1995. Influence of vegetation on the stability of slopes. In Barker, D.H. (eds.), *Vegetation and slopes*, Thomas Telford, London: 2–25.

Gasmo, J.M., Hritzuk, K.J, Rahardjo, H. & Leong, E.C. 1999. Instrumentation of an unsaturated residual soil slope. *Geotechnical Testing Journal* 22(2): 128–137.

Hillel, D. 1998. *Environmental Soil Physics*. Academic Press, San Diego, CA, USA.

Holtz, W.G. 1983. The influence of vegetation on the swelling and shrinkage of clays in the united states of America. *Géotechnique* 33(2): 159–163.

Li, J., Smith, D.W., Fityus, S.G. & Sheng, D.C. 2002. Quantitative analysis of moisture content determination in expansive soils using neutron probes. *3rd Int. Conf. on Unsaturated Soils*, Recife, Brazil. Vol. 1: 363–368.

Lim, T.T., Rahardjo, H., Chang, M.F. & Fredlund, D.G. 1996. Effect of rainfall on matric suction in a residual soil slope. *Canadian Geotechnical Journal* 33(2): 618–628.

Liu, T.H. 1997. *Problems of expansive soils in engineering construction*. Architecture and Building Press of China.

Morel-Seytoux, H.J. 1983. Infiltration affected by air, crust, ice and various sources of heterogeneity. *Advances in infiltration*, Pub l: 11–83. Am. Soc. Agric. Eng., St. Joseph, MI.

Morris, P.H., Graham, J. & Williams, D.J. 1994. Crack depths in drying clays using fracture mechanics. Fracture mechanics applied to geotechnical engineering, *Geotechnical Special Publication* 43: 41–53.

Nelson, J.D. & Miller, D.J. 1992. *Expansive soils—Problems and Practice in Foundation and Pavement Engineering.* Wiley Interscience, New York.

Ng, C.W.W. & Pang, Y.W. 2000. Experimental investigation of soil-water characteristics of a volcanic soil. *Canadian Geotechnical Journal* 37(6): 1252–1264.

Ng, C.W.W. & Zhan, L.T. 2007. Comparative study of rainfall infiltration into a bare and a grassed unsaturated expansive soil slope. *Soils and Foundations* 47(2): 207–217.

Ng, C.W.W., Zhan, L.T., Bao, C.G., Fredlund, D.G. & Gong, B.W. 2003. Performance of an unsaturated expansive soil slope subjected to artificial rainfall infiltration. *Géotechnique* 53(2): 143–157.

Ortigao, J.A.R., Lourses, R.R.T., Nogueira, C. & Alves, L.S. 1997. Slope failures in tertiary expansive OC clays. *Journal of Geotechnical and Geoenviromental Engineering* 123(9): 812–817.

Øygarden, L., Kværner, J. & Jenssen, P.D. 1997. Soil erosion via preferential flow to drainage systems in clay soils. *Geoderma* 76: 65–86.

Richard, B.G., Peter, P. & Emerson, W.W. 1983. The effect of vegetation on the swelling and shrinkage of soils in Australia. *Géotechnique* 33(2): 127–139.

Sivapullaiah, P.V., Sridharan, A. & Stalin, V.K. 1996. Swelling behavior of soil-bentonite mictures. *Canadian Geotechnical Journal* 33(5): 808–814.

Steinberg, M. 1998. *Geomembranes and The Control of Expansive Soils in Construction.* McGraw-Hill, New York.

Thetaprobe 1999. *Theta-probe—soil moisture sensor.* Delta-T Device Ltd, Cambridge, U.K.

Ward, W.H. 1953. Soil movement and weather. *Proc. 3rd Int. Conf. Soil Mech*., Zurich, Vol. 2: 477–481.

Zhan, L.T. 2003. Field and laboratory study of an unsaturated expansive soil associated with rain-induced slope instability. PhD thesis. The Hong Kong University of Science and Technology.

Zhan, L.T. Ng, C.W.W. & Fredlund, D.G. 2006. Instrumentation of an unsaturated expansive soil slope. *Geotechnical Testing Journal* 30(2): 113–123.

Zhan, L.T. Ng, C.W.W. & Fredlund, D.G. 2007. Field study of rainfall infiltration into a grassed unsaturated expansive soil slope. *Canadian Geotechnical Journal* 44(4): 392–408.